Surfaces and Interfaces 42 (2023) 103320

Contents lists available at ScienceDirect

Surfaces and Interfaces

journal homepage: www.sciencedirect.com/journal/surfaces-and-interfaces

Conditions of enhanced evaporation for nanofluids droplet and inhibition of coffee-ring effect under buoyancy and Marangoni convection

Yue-Qun Tao [a], Qiu-Sheng Liu [a,b,*]

[a] National Microgravity Laboratory, Institute of Mechanics, Chinese Academy of Sciences, Beijing 100190, China
[b] School of Engineering Science, University of Chinese Academy of Sciences, Beijing 100049, China

ARTICLE INFO

Keywords:
Nanofluid sessile droplet
Evaporation kinetics
Deposition pattern
Buoyancy convection
Marangoni convection

ABSTRACT

Evaporation of nanofluid droplets whose size is larger than capillary length is common in industrial processes, but there is currently a lack of research on the evaporation kinetics and more complex deposition patterns under the combined effects of buoyancy and Marangoni convection of large evaporating droplet. Experimental investigations on evaporation of Al_2O_3–H_2O nanofluid sessile droplet with initial contact line diameter of 4 mm on heating PTFE coating substrate are reported. The variation in contact angle, contact radius, and droplet volume over time under different conditions were obtained through experiments. The average evaporation rate is calculated. Internal flow characteristics are inferred through the surface temperature distribution detected by the top view infrared camera. The constant contact radius mode takes place at the beginning of evaporation. Then mixed evaporation mode and stick slip mode may occur for different substrate temperature, nanoparticle mass concentration and nanoparticle size. Increasing nanoparticle size causes a decrease in average evaporation rate. Whether the use of nanofluids can improve evaporation rate and heat transfer or not depends on multiple factors. Convection cells exist, and three kinds of deposition patterns are formed due to the underlying coupled transport phenomena. Under the combined effect of buoyancy and Marangoni convection in this article, the most common coffee-ring pattern does not appear. The deposition patterns are directly affected by the pinning stability, which decrease at higher temperature.

1. Introduction

Nanofluid is a new type of uniform and stable suspension, which contains solid particles with particle size less than 100 nm [1]. Nanofluid droplet evaporation is a complex heat and mass transfer physical process which takes place at gas-liquid interface. With the development of nanofluid technology, nanofluid sessile droplet evaporation is applied in a wide variety of practical industrial processes such as ink-jet printing, thin film coating, surface patterning, fabrication of DNA microarray and spray cooling, etc. [2–7]. The evaporation kinetics of nanofluids droplet and the deposition patterns after drying are two of the key issues in engineering applications and have become research hotpots in recent years [8–10]. After two decades of investigation, there are some consistent understandings. Kinetics of evaporation are closely related to motion of contact line and variation of contact angle over time. There are four typical modes in perspective of contact line behavior for sessile droplet evaporation: constant contact angle (CCA) mode, constant contact radius (CCR) mode, stick−slip mode, and mixed mode [11,12]. The typical deposition patterns after sessile nanofluid droplet drying are coffee-ring pattern, uniform pattern, stick-slip pattern, fingering structure, and combined pattern [4,13]. The Marangoni flow driven by surface tension generated by temperature gradient will affect the evaporation process and deposition pattern. Despite the consistent understandings, there are still contradictory conclusions.

The evaporation rate directly impacts the design of heat transfer equipment. However, using nanofluid to promote the evaporation performance is still ambiguous. Sefiane and Bennacer [8]carried out experimental investigations on aluminum-ethanol nanofluid sessile droplet evaporation on heating PTFE substrate. They found the addition of nanoparticles leads to a decrease in evaporation rate. Katre et al. found the lifetime of a droplet laden with 0.6 wt.% nanoparticles are consistently lower (approximately 0.6 to 0.7 times) than that of a binary droplet without nanoparticles [14]. Nanoparticles loading can enhance the pinning effect and hence increase the evaporating surface area and evaporation rate. The infrared camera images reveal richer thermal waves and complex internal flow of nanofluid droplets than pure liquid

* Corresponding author at: National Microgravity Laboratory, Institute of Mechanics, Chinese Academy of Sciences, Beijing 100190, China.
E-mail address: liu@imech.ac.cn (Q.-S. Liu).

https://doi.org/10.1016/j.surfin.2023.103320
Received 3 July 2023; Received in revised form 8 August 2023; Accepted 18 August 2023
Available online 25 August 2023

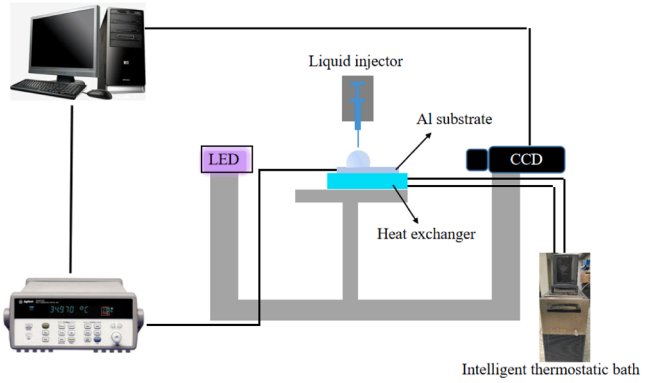

Fig. 1. The experimental setup of the optical observation, temperature control, data acquisition, droplet injection.

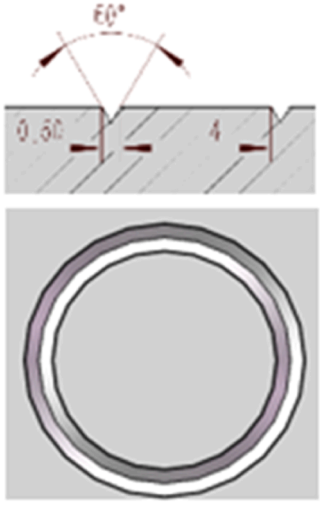

Fig. 2. The grooved substrate surface on which forms the droplet with fixed initial contact line diameter about 4 mm.

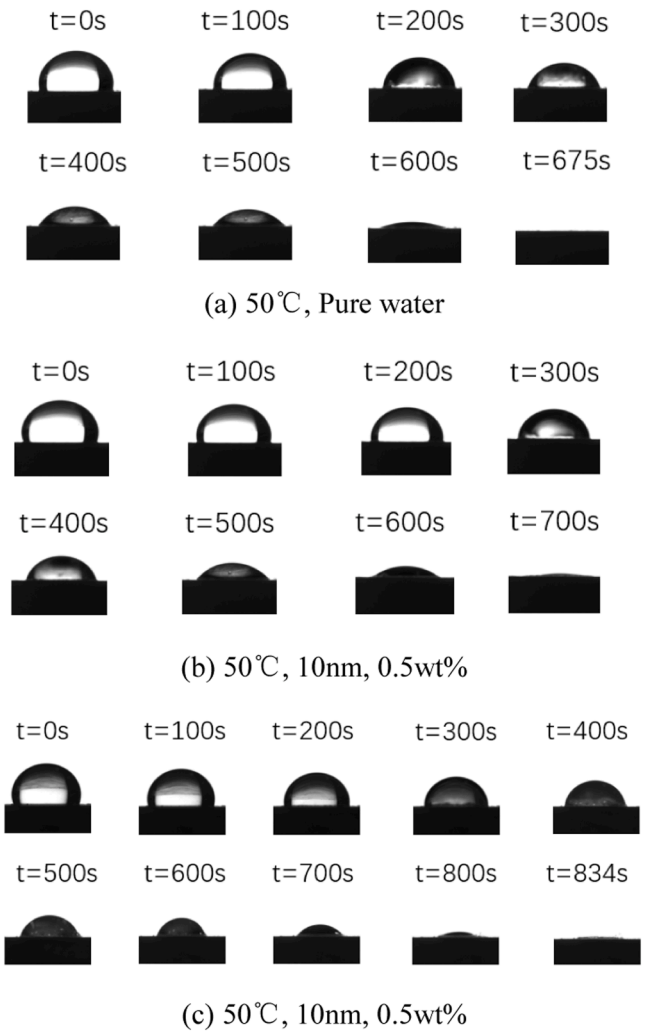

Fig. 3. The evolution of the nanofluid droplet and pure water obtained from side view CCD.

[15,16]. Chen et al. [17] found that the adding nanoparticles into base fluid can cause both higher and lower evaporation, which depends on the type of nanoparticle and the adding surfactant. Govindha et al. [18] found that the droplet contact line dynamics instead of thermal conductivity is the determining factor of evaporation rate. It is found by Zaaroura et al. [19] that the increased or decreased evaporation rate for nanofluid droplet compared with pure water is related to the surface temperature and nanoparticles size. The origin of the different behavior comes from the thermophysical properties as well as the convection caused by Marangoni effects inside droplet.

The deposition patterns and self-assembly behavior of nanofluids are also important concerns in engineering application. The surfactant [20], Marangoni flow [21], concentration and particle size [22], particle geometry [23], solid substrate temperature [24] and surface energy [25] are the known influencing factors. A series of previous studies have focused on the very common patterns of coffee ring deposition. Alexandru and Duan [20] found the existence of surfactant in nanofluids promotes the appearance of the coffee-ring pattern. Marangoni flow [21, 26] can transport the particles toward the center and thus suppress the coffee-ring effect. Ring pattern tends to form at lower concentration and smaller particle size [22]. Other researchers also found a variety of more complex structures [27–30]. The formation mechanism of other very complex deposition patterns under the combined effects of various parameters is still worth further exploration.

The evaporation rate as well as the deposition patterns depend both on the evaporation mode and the internal flow. The vast majority of the experimental investigations deal with drops having a radius less than the capillary length in which the gravity force and be ignored. However, droplet evaporation with larger dimensions than capillary length is common in industry applications. In this study, experimental investigation on evaporation of nanofluid sessile droplet on heating PTFE coating surface is conducted. With the constraint of the evaporation substrate, we obtained droplets with an initial contact line diameter of 4 mm. The objective of this work is to find out the evaporation kinetics and deposition characteristics under the joint effect of evaporation, gravity induced buoyancy flow and thermal Marangoni flow. Effects of substrate temperature, particle size, nanofluid concentration and substrate conductivity are analyzed.

2. Experimental setup and procedure

2.1. Experimental setup

The experimental setup is depicted in Fig. 1. The droplet evaporation process takes place on the aluminum cylinder substrate with PTFE coating. The substrate surface is patterned with a trench as shown in Fig. 2, which makes it possible to form the desired size of droplet with fixed initial contact line diameter of 4 mm. Without the groove, the contact line diameter will be larger than 4 mm and the height will be lower at volume of 20 uL (See Supplementary Material Fig. S1).

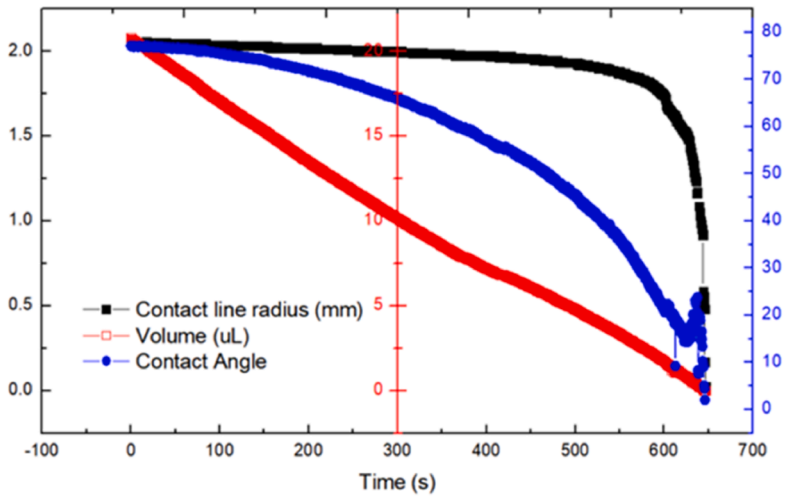

(a) 50℃, Pure water

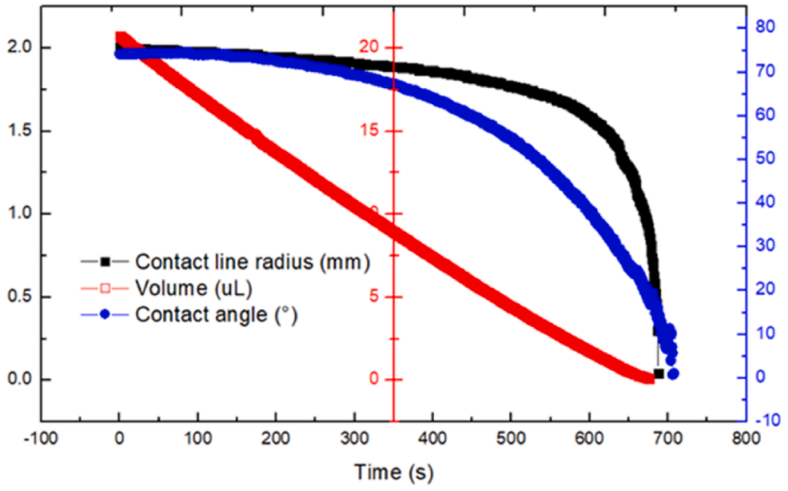

(b) 50℃, 10nm, 0.5wt%

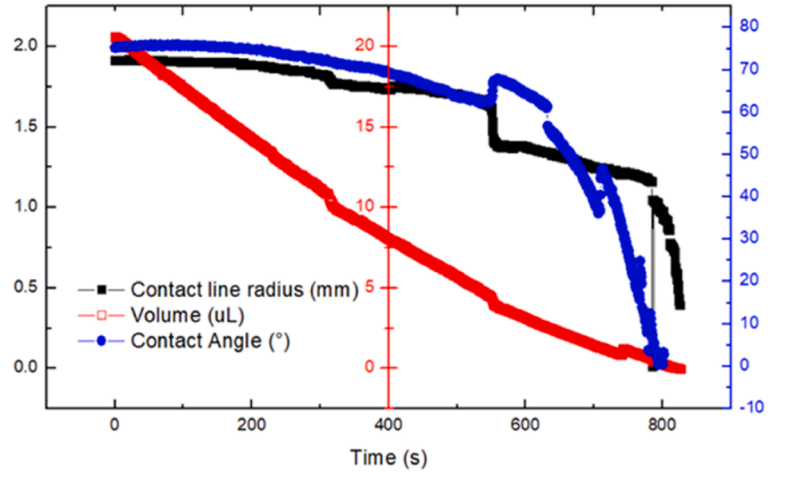

(c) 50℃, 50nm, 0.5wt%

Fig. 4. Variation of contact angle, contact line radius, and volume with time obtained by side view CCD images analysis.

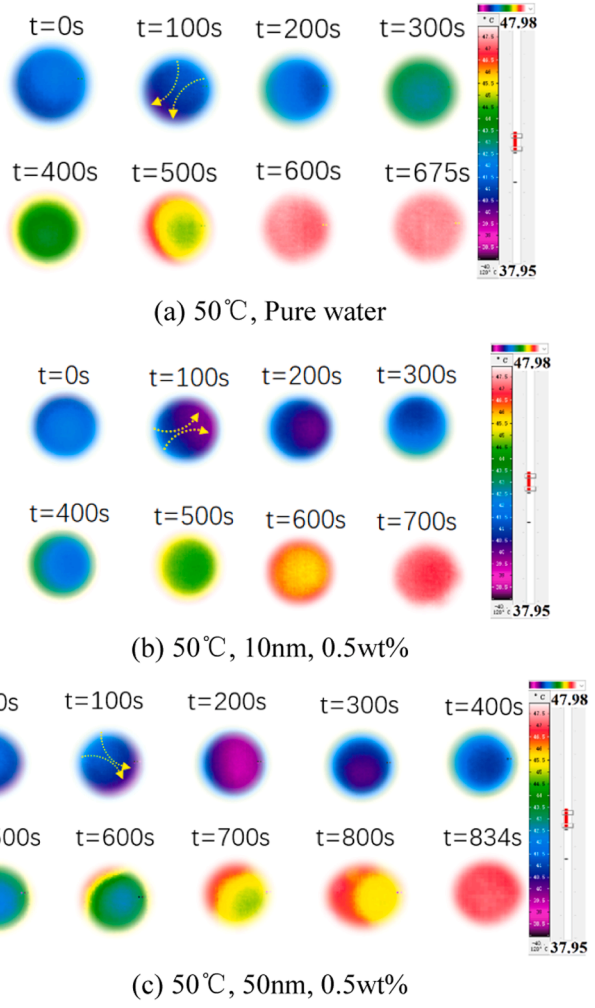

Fig. 5. The droplet surface temperature distribution obtained by top view Infrared camera observation (The temperature is in the range of 37.95 °C~ 47.98 °C).

Therefore, we use the groove to get a higher droplet and to better study the effect of gravity induced buoyancy flow. The cylinder substrate is put on a cold plate heat exchanger. Circulating water with temperature in the range of 30~70 °C is used to control the temperature of the cylinder substrate. Two T-type thermocouples are attached to the substrate surface to monitor the accurate temperature. The instantaneous morphology of the droplet is obtained by Dasla-m128 CCD from side view (2fps, 1216 × 1216 pixels). The surface temperature of the droplet is recorded by an Infra-Tec infrared camera from the top view (2fps, 1216 × 1216 pixels). The deposition pattern after drying is observed by Leica 2700 M microscope. The droplet is created using a micro-pipette by gently laying down the droplet on the substrate. In the present study, the initial volume is 20 micro-liters. The substrate is cleaned in ultrasonic water bath before each experiment and reused after drying. All the experiments were repeated 2~3 times to ensure the reproducibility of the results.

2.2. Materials

Al_2O_3—H_2O nanofluid of 20 wt% is purchased from SEEDIOR Company(Phase γ, purity: 99.9%). We dilute it with pure water to a specific fraction and make it homogeneous using a magnetic stirrer. Before each experiment, we use a magnetic stirrer to stir the nanofluid for 10 min to ensure uniformity of nanofluids. No visible settlement aggregation phenomenon takes place before each experiment. Three kinds of nanofluid are used with average nanoparticle sizes 5–10, 20 and 50 nm.

2.3. Analysis

Each image (interval time 0.5 s) is analyzed to get the instantaneous values of droplet volume, contact line radius, as well as contact angle. The exponential fitting method is used to fit the droplet morphology, and the volume is calculated based on the assumption of axial symmetry. The convection characteristic is monitored according to the temperature distribution which is obtained by the top-view infrared camera. The deposition pattern is observed by Leica 2700 M microscope using 5x lens.

3. Results and discussion

3.1. Evaporation kinetics

The evolution of nanofluid droplet and pure water from side view are shown in Fig. 3. The entire lifetime of the pure water droplet is 675 s. While for nanofluid with particle size of 10 and 50 nm, it is 703 and 834 s, respectively. Adding nanoparticles to the solution reduces the evaporation rate under these two conditions. However, this impact is not universal. Previous investigations also found both enhanced and slowed down evaporation processes [17]. This is the result of multiple factors working together, and we will further analyze it later in Section 3.4.

By processing each image, we obtained the changes in droplets' contact angle, contact line radius, and volume along with time. As is shown in Fig. 4, the constant contact radius (CCR) mode first occurs at the first stage of evaporation. Then different evaporation processes take place. The mixture evaporation mode follows for pure water and nanofluid with particle size of 10 nm. However, nanofluid with 50 nm nanoparticles inside shows stick-slip behavior. The decrease of the contact angle results in the increase of the interface energy and once it exceeds the energy barrier, the contact line slips to dissipate the exceeded energy. On the one hand, the deposition of nanoparticles enhances the contact line pinning effect of droplet, namely the pinning stick behavior. On the other hand, the viscosity of nanofluid is also higher compared with pure water, which leads to the re-pinning process after the first stage of depinning. The volume of pure liquid changes linearly with time, which is not applicable for nanofluids when stick-slip behavior takes place. The contact radius directly determines the evaporation rate. Droplets with longer first pining stage have higher evaporation rate.

3.2. Thermal convection inside droplet

Fig. 5 depicts the temperature distribution of the droplet surface. The diameter of the droplet is larger than that of the capillary length, so gravity induced buoyancy convection cannot be ignored. Besides, there is also Marangoni convection caused by surface tension temperature gradient at the interface of droplet. The convection cells exist in the early stage and then disappear after a period. In previous results of Katre's et al. [31] using a critically inclined heated surface also reveals similar flow pattern, in which the buoyancy and Marangoni convection both plays important roles as well.

Three relevant dimensionless numbers, i.e. Marangoni number, Rayleigh number and Bond number are calculated to show the driving phenomenon. γ is the surface tension coefficient. ΔT is the temperature difference between the substrate and the room temperature. L is the radial dimensions of the droplet. η, α, ν, β, are respectively the dynamic viscosity, thermal diffusivity, kinematic viscosity, and volume expansivity. g is the gravitational constant. The thermophysical parameters of nanofluid with different mass fractions, nanoparticles size and temperature are obtained according to the previous research results [32–36] as shown in supplementary material. Fig. 6 shows the results of the specific three cases of the variation of dimensionless numbers with time. The

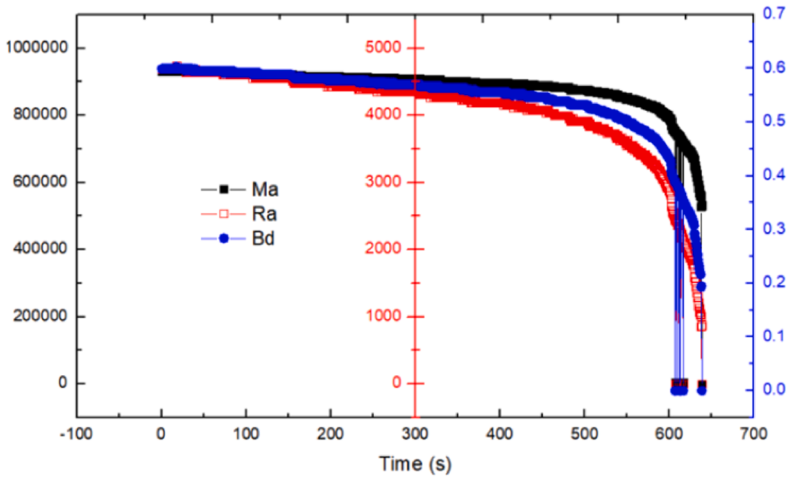

(a)

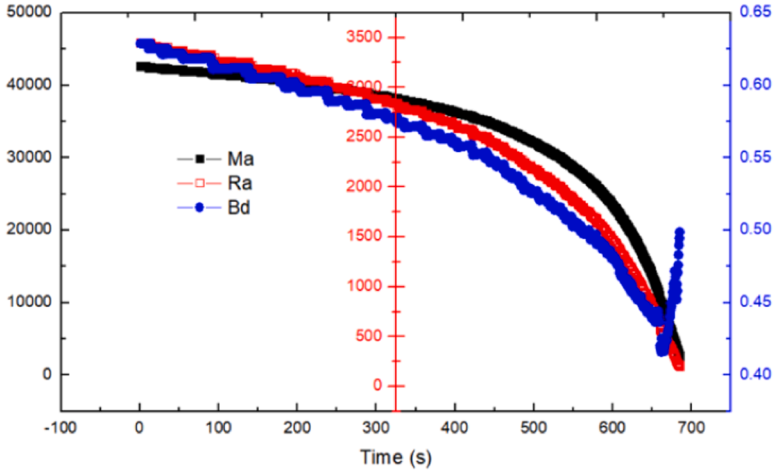

(b)

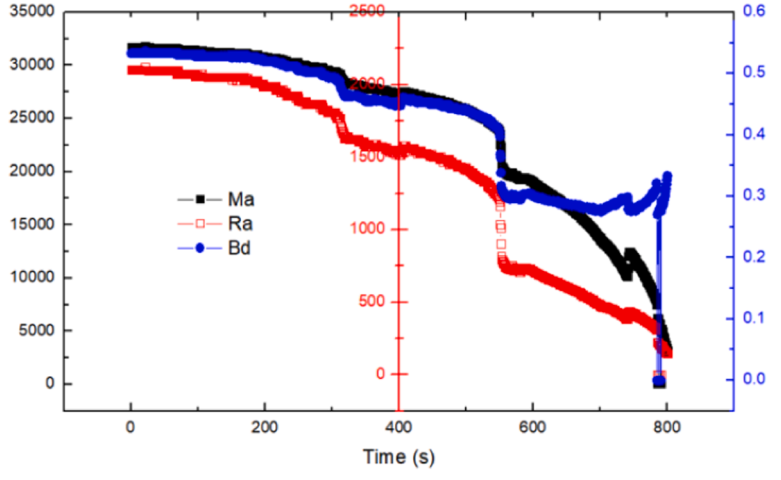

(c)

Fig. 6. The variation of dimensionless number with time at heating temperature 50 °C: (a) Pure water; (b) 10 nm, Initial concentration 0.5% wt. (c) 50 nm, Initial concentration 0.5wt%.

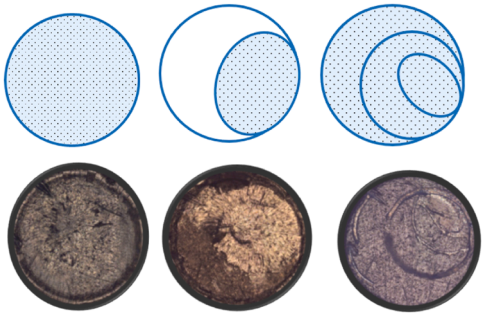

Fig. 7. The deposition patterns observed by microscope using 5x lens:(a)Ring-disk; (b)Combined pattern;(c) Stick-slip pattern.

Table 1
The lifetime of the droplet(pure water and 0.5% wt nanofluid).

Heating Temperature (°C)	Lifetime (s) Base fluid	Lifetime (s) 10nm	Lifetime (s) 20nm	Lifetime (s) 50nm
30	2622±3	2305±5	2632±5	2985±8
40	1250±3	1210±5	1274±4	1515±6
50	675±3	703±5	722±4	834±7
60	411±2	378±5	421±5	434±5
70	306±2	279±3	292±4	314±5

variation of the thermophysical parameters is accounted for. The initial Bd number is in the range of 0.5~0.65, which indicates that the capillary forces and gravity force both play important roles at the early evaporation stage. The Rayleigh and Marangoni numbers indicate that there exists the thermocapillary-buoyancy convection. The dimensionless numbers of Ma and Ra decrease with the evaporating time and hence both Marangoni effect and buoyancy effect weaken.

$$Ma = -\frac{d\gamma}{dT}\frac{L\Delta T}{\eta\alpha} \tag{1}$$

$$Ra = Pr{\cdot}Gr = \frac{v}{\alpha}\frac{g\beta L^3\Delta T}{v^2} \tag{2}$$

$$Bd = \frac{\rho g L^2}{\gamma} \tag{3}$$

3.3. The deposition pattern after drying

As shown in Fig. 7, three kinds of deposition patterns are formed. We do not observe the very typical coffee ring structure. It is worth noting that the pinning effect is enhanced through the groove on the substrate, which would have promoted the formation of the most common coffee rings. However, disks covering the entire 4 mm diameter area, or only occupying a smaller area, circular or irregularly shaped can be always found. The contact line motion of the droplets is the decisive factor of the deposition pattern. The deposition of the disk is reflection of the Marangoni and buoyancy flow, which takes the nanoparticles away from the contact line and leads to the formation of disks. These deposition patterns of disk in present study show that thermocapillary-buoyancy convection has important impact in all experiments.

3.4. Effects of heating temperature, nanoparticle size and concentration

Effects of heating temperature and nanoparticle size on the lifetime of pure water and nanofluid droplet are shown in Table 1. The contact line and contact angle versus the experiment duration and the lifetime for different temperature and particle size are given in Supplementary Material 1. The evaporation rates are most strongly affected by the substrate temperature, which is consistent with previous research results [37]. Increasing nanoparticle size leads to a longer lifetime and lower average evaporation rate. One of the underlying reasons for the observed phenomenon is that the thermal conductivity increment for evaporation process under conditions of higher temperature and smaller particle size is higher [38]. Similar result that smaller nanoparticles show better performance in evaporation enhancement was also found in Ref. [19]. Whether the use of nanofluids can improve evaporation rate

Table 2
The deposition pattern and dimensionless numbers under different conditions.

Name U nit	Temperature °C	Particle size nm	Concentration wt%	Ma	Ra	Bd	Deposition pattern
1.	30	10	0.5	3322	267	0.61	Ring-disk
2.	30	20	0.5	3149	247	0.60	Ring-disk
3.	30	50	0.5	2725	199	0.57	Ring-disk
4.	40	10	0.5	18,668	1495	0.61	Combined
5.	40	20	0.5	17,563	1371	0.60	Ring-disk
6.	40	50	0.5	14,946	1086	0.57	Ring-disk
7.	50	10	0.5	42,471	3388	0.62	Combined
8.	50	20	0.5	39,598	3078	0.61	Combined
9.	50	50	0.5	33,054	2392	0.58	Combined
10.	60	10	0.5	78,008	6194	0.63	Combined
11.	60	50	0.5	58,700	4228	0.59	Combined
12.	70	10	0.5	130,340	10,293	0.64	Stick-slip
13.	70	20	0.5	118,558	9122	0.63	Stick-slip
14.	70	50	0.5	94,158	6745	0.60	Stick-slip
15.	70	20	0.1	124,475	9444	0.62	Stick-slip
16.	70	20	0.5	118,558	9122	0.63	Stick-slip
17.	70	20	1	111,988	8772	0.64	Stick-slip
18.	60	20	0.1	75,093	5729	0.61	Stick-slip
19.	60	20	0.5	71,934	5565	0.62	Combined
20.	60	20	1	68,379	5384	0.63	Combined
21.	50	20	0.1	41,144	3154	0.60	Stick-slip
22.	50	20	0.5	39,598	3078	0.61	Stick-slip
23.	50	20	1	37,838	2993	0.62	Combined
24.	30	–	Water	8570	414	0.55	–
25.	40	–	Water	44,046	2118	0.56	–
26.	50	–	Water	90,876	4352	0.57	–
27.	60	–	Water	149,812	7140	0.58	–
28.	70	–	Water	168,814	8002	0.59	–

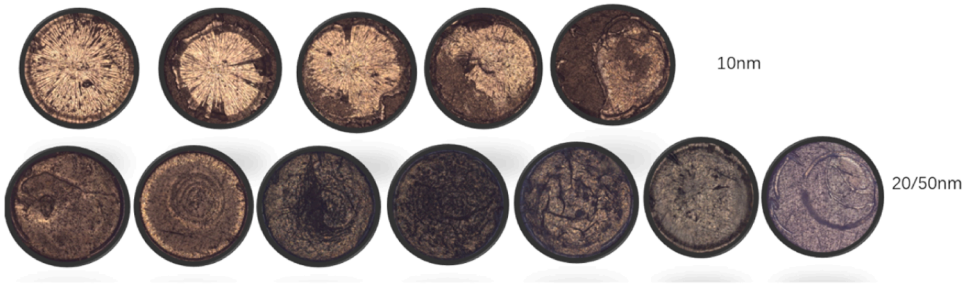

Fig. 8. The deposition patterns for nanofluid droplets containing different particle sizes observed by microscope using 5x lens.

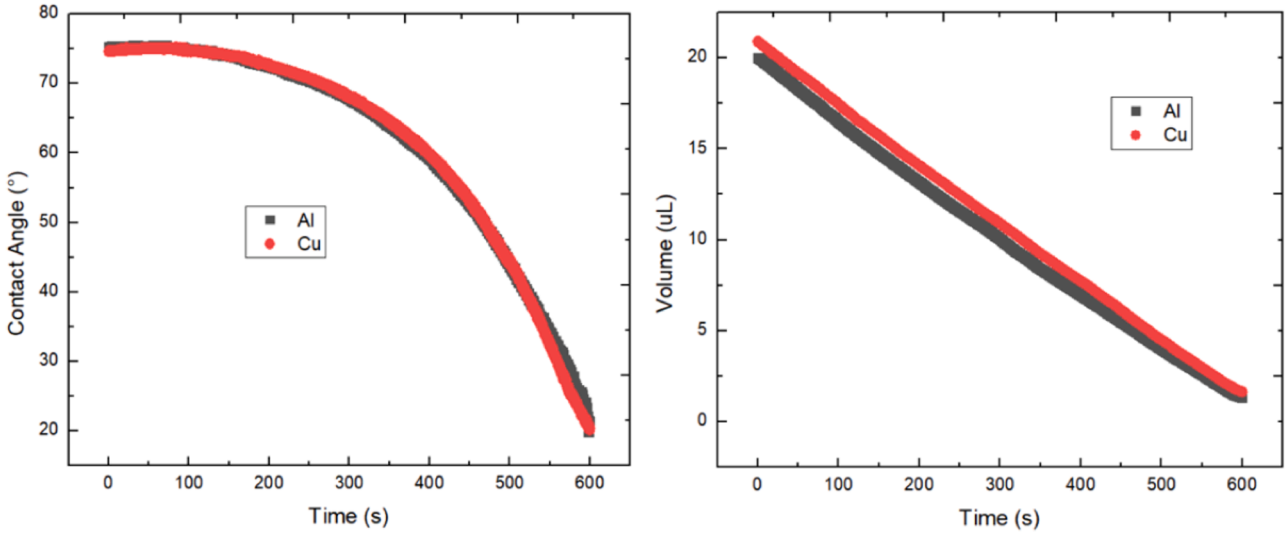

Fig. 9. Effect of substrate conductivity on the variation of contact angle and droplet volume obtained by side view CCD image analysis.

and heat transfer or not depends on temperature as well as particle size. The evaporation rate of nanofluid droplet with 50 nm nanoparticles is always lower than that of pure water at same temperature. The addition of 20 nm nanoparticles enhances the evaporation rate at temperature of 70 °C but decreases the evaporation rate at lower temperature.

Table 2 summarizes the results obtained under different experimental conditions. The initial dimensionless numbers are also listed. Overall, the deposition patterns are the joint results of particle size, concentration as well as the substrate temperature, instead of solely factor. Stick-slip pattern is more likely to take place at higher temperature and lower concentration; Ring-disk pattern occurs at lower temperature and higher concentration. *Ra* and *Ma* numbers increase with the increasing temperature, which results in the more intense internal flow. Therefore, increasing the substrate heating temperature will increase instability of the contact line, which facilitates the formation of combined and stick-slip pattern. Besides, as shown in Fig. 8, we also discovered some interesting deposition patterns during the investigation. The deposition pattern in the disk formed after 20 and 50 nm nanofluid droplet drying is randomly distributed. But for 10 nm nanofluid, it shows the radial radiation stripe structure. When evaporation is almost complete, a gelation film is formed at the high nanoparticle concentration. As the droplets continue to evaporate, tensile stress is generated by the shrinking effect at the edge where the fastest evaporation occurs. At the same time, there is adhesion stress between the sessile droplet and the solid substrate. Once the local tensile stress exceeds the adhesion stress, the local cracks forms in the radial direction and the observed special deposition pattern forms. It is evident that the tensile force in droplets containing 10 nm nanoparticles is stronger as compared to droplets containing larger nanoparticles. Previous studies have reported a similar crack deposition pattern [13]. The results in this present study have clarified the effects of particle size. For further applications which desire uniform coatings, it suggests using nanoparticles with larger sizes to avoid the formation of cracks.

3.5. *Effects of substrate conductivity*

The evaporation processes which take place on solid substrate made of copper and aluminum with PTFE coatings are investigated. The conductivity of copper is 397 W/m·K and the conductivity of aluminum is 237 W/m·K. The conductivity values of these two kinds of materials differ by a factor of 1.7. As is shown in Fig. 9, there is no obvious difference in the contact angle, contact line, and volume variation of droplets on these two selected substrates. For these two metals with high thermal conductivity, thermal conductivity is not the main influencing factor in the evaporation process. Due to the consistent contact wetting behavior on the surface of the PTFE coatings, the evaporation kinetics displays no difference in present study. Previous study [34] found that an increase in thermal conductivity accelerates evaporation, in cases where there is a significant difference in thermal conductivity. If we continue to enlarge the differences in substrate thermal conductivity to magnitude, whether there are differences remains to be discussed.

6. Conclusions

Evaporation of Al_2O_3–H_2O nanofluid sessile droplet with initial contact line radius 4 mm on PTFE coating substrate is experimentally investigated in this paper. Different from previous research on small-scale droplets [8,24,39,40], both the Marangoni flow and buoyancy flow play important roles in present cases. We calculated the diameter, contact angle, and volume of droplets based on the central symmetry

assumption by processing two-dimensional CCD images. Different pinning-depinning behavior takes place under the joint effects of substrate temperature, concentration, and nanoparticle size. Smaller particles and higher substrate temperature are the favorable factors for nanofluid to promote evaporation process as compared with pure water. Due to the combined action of Marangoni flow and buoyancy flow, there is always disks deposition pattern in present investigation. The orderly arrangement after nanofluid droplet drying which contains 10 nm size of nanoparticles is due to the surpass of edge tensile stress to the substrate adhesion stress. It suggests using nanoparticles with larger sizes to avoid the formation of radial crack deposition.

CRediT authorship contribution statement

Yue-Qun Tao: Conceptualization, Methodology, Investigation, Writing – original draft, Visualization, Funding acquisition. **Qiu-Sheng Liu:** Conceptualization, Supervision, Validation, Writing – review & editing, Project administration, Funding acquisition.

Declaration of Competing Interest

The authors declare that they have no known competing financial interests or personal relationships that could have appeared to influence the work reported in this paper.

Data availability

Data will be made available on request.

Acknowledgment

This work was financially supported by China Manned Space Program (CSS-MT), Bureau of International Cooperation of Chinese Academy of Sciences (No.115111KYSB2020008), the Science and Technology Innovation 2025 Major Project of Ningbo City (Grant No. 2022Z213), the National Natural Science Foundation of China (Grants No. 11532015).

Supplementary materials

Supplementary material associated with this article can be found, in the online version, at doi:10.1016/j.surfin.2023.103320.

References

[1] H. Riazi, T. Murphy, G.B. Webber, R. Atkin, S.S.M. Tehrani, R.A. Taylor, Specific heat control of nanofluids: a critical review, Int. J. Therm. Sci. 107 (2016) 25–38, https://doi.org/10.1016/j.ijthermalsci.2016.03.024.
[2] M. Amjad, Y. Yang, G. Raza, H. Gao, J. Zhang, L. Zhou, X. Du, D. Wen, Deposition pattern and tracer particle motion of evaporating multi-component sessile droplets, J. Colloid Interface Sci. 506 (2017) 83–92, https://doi.org/10.1016/j.jcis.2017.07.025.
[3] M. Janocha, E. Tsotsas, Coating layer formation from deposited droplets: a comparison of nanofluid, microfluid and solution, Powder Technol. 399 (2022), 117202, https://doi.org/10.1016/j.powtec.2022.117202.
[4] X. Zhong, A. Crivoi, F. Duan, Sessile nanofluid droplet drying, Adv. Colloid Interface Sci. 217 (2015) 13–30, https://doi.org/10.1016/j.cis.2014.12.003.
[5] G. Duursma, K. Sefiane, A. Kennedy, Experimental studies of nanofluid droplets in spray cooling, Heat Transfer Eng. 30 (2009) 1108–1120, https://doi.org/10.1080/01457630902922467.
[6] D. Sabourin, J. Petersen, D. Snakenborg, M. Brivio, H. Gudnadson, A. Wolff, M. Dufva, Microfluidic DNA microarrays in PMMA chips: streamlined fabrication via simultaneous DNA immobilization and bonding activation by brief UV exposure, Biomed. Microdevices 12 (2010) 673–681, https://doi.org/10.1007/s10544-010-9420-7.
[7] A.A. Mehrizi, H. Karimi-maleh, M. Naddafi, O. Karaman, F. Karimi, C. Karaman, C. K. Cheng, Evaporation characteristics of nanofuel droplets: a review, Fuel 319 (2022), 123731, https://doi.org/10.1016/j.fuel.2022.123731.
[8] K. Sefiane, R. Bennacer, Nanofluids droplets evaporation kinetics and wetting dynamics on rough heated substrates, Adv. Colloid Interface Sci. 147-148 (2009) 263–271, https://doi.org/10.1016/j.cis.2008.09.011.
[9] P. Chen, S. Harmand, S. Szunerits, R. Boukherroub, Evaporation behavior of PEGylated graphene oxide nanofluid droplets on heated substrate, Int. J. Therm. Sci. 135 (2019) 445–458, https://doi.org/10.1016/j.ijthermalsci.2018.06.030.
[10] C.H. Chon, S. Paik, J.B. Tipton, K.D. Kihm, Effect of nanoparticle sizes and number densities on the evaporation and dryout characteristics for strongly pinned nanofluid droplets, Langmuir 23 (2007) 2953–2960, https://doi.org/10.1021/la061661y.
[11] A.G. Sourais, I.E. Markodimitrakis, N.T. Chamakos, A.G. Papathanasiou, Droplet evaporation dynamics on heterogeneous surfaces: numerical modeling of the stick-slip motion, Int. J. Heat Mass. Transf. 207 (2023), 123992, https://doi.org/10.1016/j.ijheatmasstransfer.2023.123992.
[12] N.M. Kovalchuk, A. Trybala, V.M. Starov, Evaporation of sessile droplets, Curr. Opin. Colloid Interface Sci. 19 (2014) 336–342, https://doi.org/10.1016/j.cocis.2014.07.005.
[13] M. Parsa, S. Harmand, K. Sefiane, Mechanisms of pattern formation from dried sessile drops, Adv. Colloid Interface Sci. 254 (2018) 22–47, https://doi.org/10.1016/j.cis.2018.03.007.
[14] P. Katre, S. Balusamy, S. Banerjee, L.D. Chandrala, K.C. Sahu, Evaporation dynamics of a sessile droplet of binary mixture laden with nanoparticles, Langmuir 37 (2021) 6311–6321, https://doi.org/10.1021/acs.langmuir.1c00806.
[15] P. Katre, S. Balusamy, S. Banerjee, K.C. Sahu, An experimental investigation of evaporation of ethanol–water droplets laden with alumina nanoparticles on a critically inclined heated substrate, Langmuir 38 (2022) 4722–4735, https://doi.org/10.1021/acs.langmuir.2c00306.
[16] P. Katre, S. Banerjee, S. Balusamy, K.C. Sahu, Stability and retention force factor for binary-nanofluid sessile droplets on an inclined substrate, Ind. Eng. Chem. Res. (2023), https://doi.org/10.1021/acs.iecr.3c00160, 10.1021/acs.iecr.3c00160.
[17] R.H. Chen, T.X. Phuoc, D. Martello, Effects of nanoparticles on nanofluid droplet evaporation, Int. J. Heat Mass Transf. 53 (2010) 3677–3682, https://doi.org/10.1016/j.ijheatmasstransfer.2010.04.006.
[18] A.H. Govindha, P. Katre, S. Balusamy, S. Banerjee, K.C. Sahu, Counter-intuitive evaporation in nanofluids droplets due to stick-slip nature, Langmuir 38 (2022) 15361–15371, https://doi.org/10.1021/acs.langmuir.2c02590.
[19] I. Zaaroura, S. Harmand, J. Carlier, M. Toubal, A. Fasquelle, B. Nongaillard, Experimental studies on evaporation kinetics of gold nanofluid droplets: influence of nanoparticle sizes and coating on thermal performance, Appl. Therm. Eng. 183 (2021), 116180, https://doi.org/10.1016/j.applthermaleng.2020.116180.
[20] A. Crivoi, F. Duan, Effect of surfactant on the drying patterns of graphite nanofluid droplets, J. Phys. Chem. B 117 (2013) 5932–5938, https://doi.org/10.1021/jp401751z.
[21] D. Wang, P. Cheng, Nanoparticles deposition patterns in evaporating nanofluid droplets on smooth heated hydrophilic substrates: a 2D immersed boundary-lattice Boltzmann simulation, Int. J. Heat Mass Transf. 168 (2021), 120868, https://doi.org/10.1016/j.ijheatmasstransfer.2020.120868.
[22] H.H. Lee, S.C. Fu, C.Y. Tso, C.Y.H. Chao, Study of residue patterns of aqueous nanofluid droplets with different particle sizes and concentrations on different substrates, Int. J. Heat Mass Transf. 105 (2017) 230–236, https://doi.org/10.1016/j.ijheatmasstransfer.2016.09.093.
[23] A. Askounis, K. Sefiane, V. Koutsos, M.E.R. Shanahan, Effect of particle geometry on triple line motion of nano-fluid drops and deposit nano-structuring, Adv. Colloid Interface Sci. 222 (2015) 44–57, https://doi.org/10.1016/j.cis.2014.05.003.
[24] X. Zhong, F. Duan, Disk to dual ring deposition transformation in evaporating nanofluid droplets from substrate cooling to heating, Phys. Chem. Chem. Phys. 18 (2016) 20664–20671, https://doi.org/10.1039/C6CP03231A.
[25] F. Carle, D. Brutin, How surface functional groups influence fracturation in nanofluid droplet dry-outs, Langmuir 29 (2013) 9962–9966, https://doi.org/10.1021/la401428v.
[26] J. Ren, A. Crivoi, F. Duan, Disk-ring deposition in drying a sessile nanofluid droplet with enhanced marangoni effect and particle surface adsorption, Langmuir 36 (2020) 15064–15074, https://doi.org/10.1021/acs.langmuir.0c02607.
[27] E. Pauliac-Vaujour, A. Stannard, C.P. Martin, M.O. Blunt, I. Notingher, P. J. Moriarty, I. Vancea, U. Thiele, Fingering instabilities in dewetting nanofluids, Phys. Rev. Lett. 100 (2008), 176102, https://doi.org/10.1103/PhysRevLett.100.176102.
[28] I. Vancea, U. Thiele, E. Pauliac-Vaujour, A. Stannard, C.P. Martin, M.O. Blunt, P. J. Moriarty, Front instabilities in evaporatively dewetting nanofluids, Phys. Rev. E 78 (2008), 041601, https://doi.org/10.1103/PhysRevE.78.041601.
[29] P. Wąsik, C. Redeker, T.G. Dane, A.M. Seddon, H. Wu, W.H. Briscoe, Hierarchical surface patterns upon evaporation of a ZnO nanofluid droplet: effect of particle morphology, Langmuir 34 (2018) 1645–1654, https://doi.org/10.1021/acs.langmuir.7b03854.
[30] A. Crivoi, F. Duan, Evaporation-induced branched structures from sessile nanofluid droplets, J. Phys. Chem. C 117 (2013) 7835–7843, https://doi.org/10.1021/jp312021w.
[31] P. Katre, P. Gurrala, S. Balusamy, S. Banerjee, K.C. Sahu, Evaporation of sessile ethanol-water droplets on a critically inclined heated surface, IJMF 131 (2020), 103368, https://doi.org/10.1016/j.ijmultiphaseflow.2020.103368.
[32] L. Kolsi, E. Lajnef, W. Aich, A. Alghamdi, M.A. Aichouni, M.N. Borjini, H. Ben Aissia, Numerical investigation of combined buoyancy-thermocapillary convection and entropy generation in 3D cavity filled with Al_2O_3 nanofluid, Alex. Eng. J. 56 (2017) 71–79, https://doi.org/10.1016/j.aej.2016.09.005.
[33] J. Chinnam, D.K. Das, R.S. Vajjha, J.R. Satti, Measurements of the surface tension of nanofluids and development of a new correlation, Int. J. Therm. Sci. 98 (2015) 68–80, https://doi.org/10.1016/j.ijthermalsci.2015.07.008.
[34] A.N. Sterlyagov, M.I. Nizovtsev, The experimental study of evaporation of water and nanofluid droplets on the surfaces of materials with different thermal

conductivities, Colloid J. 85 (2023) 80–86, https://doi.org/10.1134/S1061933X22600543.
[35] E.B. Elcioglu, A. Guvenc Yazicioglu, A. Turgut, A.S. Anagun, Experimental study and Taguchi analysis on alumina-water nanofluid viscosity, Appl. Therm. Eng. 128 (2018) 973–981, https://doi.org/10.1016/j.applthermaleng.2017.09.013.
[36] J. Qin, Y. Tao, Q. Liu, Z. Li, Z. Zhu, N. He, Experimental and theoretical studies of different parameters on the thermal conductivity of nanofluids, Micromachines 14 (2023), https://doi.org/10.3390/mi14050964 (Basel).
[37] P. Gurrala, P. Katre, S. Balusamy, S. Banerjee, K.C. Sahu, Evaporation of ethanol-water sessile droplet of different compositions at an elevated substrate temperature, Int. J. Heat Mass Transf. 145 (2019), 118770, https://doi.org/10.1016/j.ijheatmasstransfer.2019.118770.
[38] T.P. Teng, Y.H. Hung, T.C. Teng, H.E. Mo, H.G. Hsu, The effect of alumina/water nanofluid particle size on thermal conductivity, Appl. Therm. Eng. 30 (2010) 2213–2218, https://doi.org/10.1016/j.applthermaleng.2010.05.036.
[39] W.J. Gerken, A.V. Thomas, N. Koratkar, M.A. Oehlschlaeger, Nanofluid pendant droplet evaporation: experiments and modeling, Int. J. Heat Mass Transf. 74 (2014) 263–268, https://doi.org/10.1016/j.ijheatmasstransfer.2014.03.031.
[40] I. Zaaroura, M. Toubal, H. Reda, J. Carlier, S. Harmand, R. Boukherroub, A. Fasquelle, B. Nongaillard, Evaporation of nanofluid sessile drops: infrared and acoustic methods to track the dynamic deposition of copper oxide nanoparticles, Int. J. Heat Mass Transf. 127 (2018) 1168–1177, https://doi.org/10.1016/j.ijheatmasstransfer.2018.07.102.